

Chapter 2

Building the Magneto Optic Trap: Experimental Details

This chapter describes the procedure followed for building a MOT for Rb. It begins with a discussion of the external cavity diode lasers that we built, and also the allied electronics modules. The process of active frequency stabilization is described, followed by a description of the optics layout for the MOT. This is followed by a description of the construction of the MOT chamber and its evacuation. Finally, the steps leading to the formation of the cold cloud are detailed.

The relevant transitions in Rb are in the near infrared ($\sim 780\text{nm}$). Diode lasers provide a very convenient source at this wavelength. They can be operated in single mode, are tunable, extremely compact and easy to handle.

The diode laser is a solid state device, typically made of GaAlAs. The active medium is the depletion layer at the pn junction, which has typical dimensions of length $300\mu\text{m}$, width $20\mu\text{m}$ and thickness $3\mu\text{m}$. Lasing is induced by forward biasing the diode. Electrons from the n-side move towards p-side and holes from p- side towards n-side (see figure 2.1). In the depletion layer they recombine to give light, the frequency of which depends on the bandgap. The gain profile of emission of a diode has a typical bandwidth of 10nm (see figure 2.2).

As the active medium has dimensions of a few microns, it causes the output beam to diffract from the slit-like output facets. Hence an elliptical and highly diverging beam is obtained (see figure 2.3). The cleaved faces constitute the cavity mirrors for the bare diode laser. Thus, though the gain profile is broad and continuous, only those wavelengths within

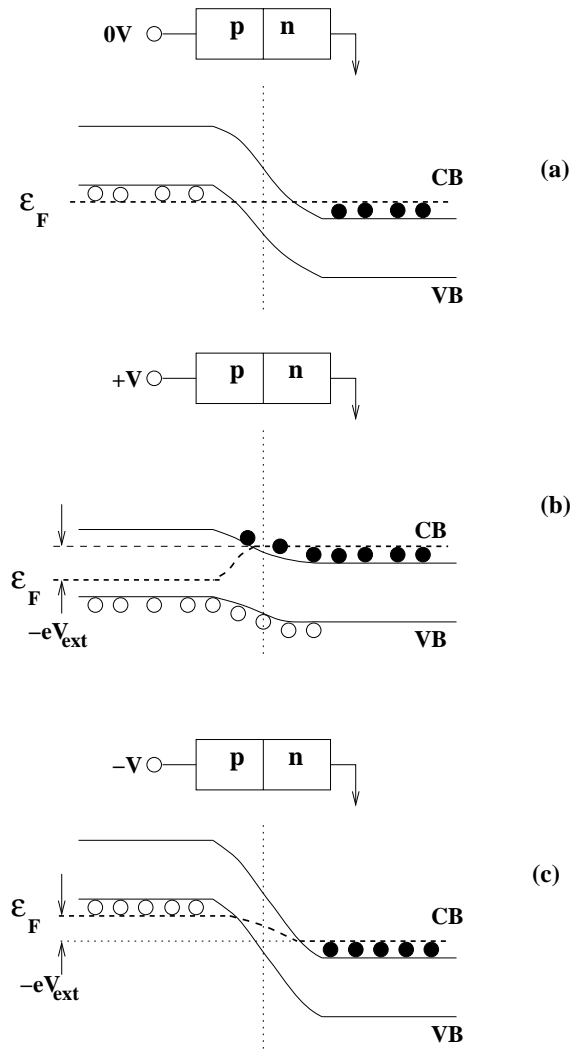


Figure 2.1: Free charge carriers at a pn junction. (a) Zero-bias equilibrium. At the interface, electrons diffuse into the p-doped area and holes into the n doped area, where they recombine. At the barrier, a layer is depleted of charge carriers and an electrical field is generated, counteracting any further diffusion. (b) At forward bias, a current flows through the junction, electrons and holes flood the barrier layer and cause recombination radiation. (c) At reverse bias, the depletion zone is enlarged. This figure is based on the reference [1].

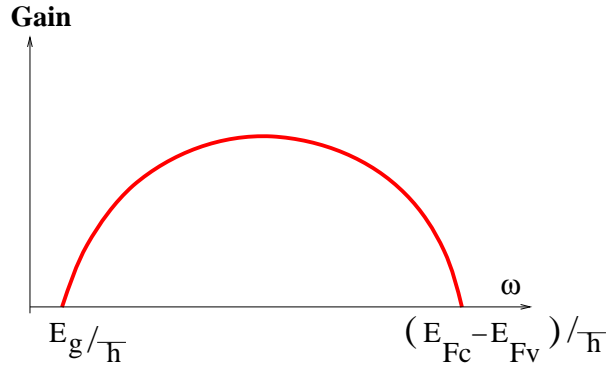


Figure 2.2: The schematic of the spectral gain profile. Amplification of light can be achieved for frequencies, in the range E_g/\hbar to $(E_{Fc} - E_{Fv})/\hbar$, where E_g is the energy difference between the conduction and valence band, E_{Fc} and E_{Fv} are the Fermi energy in the conduction and valence bands.

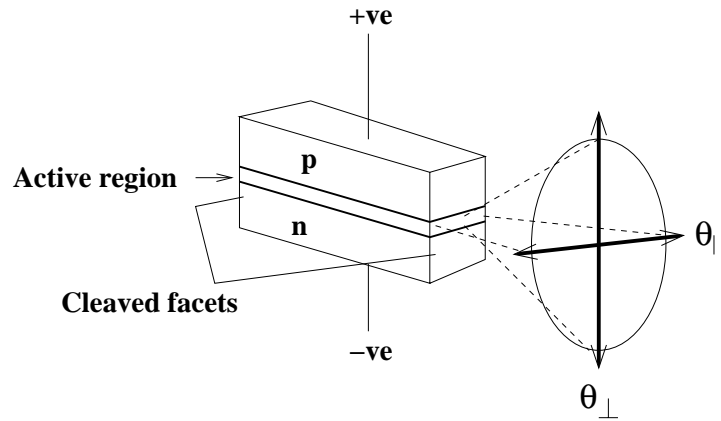


Figure 2.3: Laser diode, the light emission and beam shape.

this profile build up that satisfy the resonance condition for the cavity, ie,

$$2\lambda = mln, \tag{2.1}$$

where m is whole number, n the refractive index, and l the cavity length . The output, especially at low operating currents, is thus multimode, with the mode spacing $\frac{c}{2l} \approx 5.0 \times 10^{12}$ Hz. As the current increases the gain narrowing occurs, and fewer modes appear (figure 2.4). In laser cooling experiments, it is essential that the laser operate in a single mode. The frequency of the laser light may be altered by changing the temperature or the current. These change the bandgap and the number of free charge carriers. The temperature

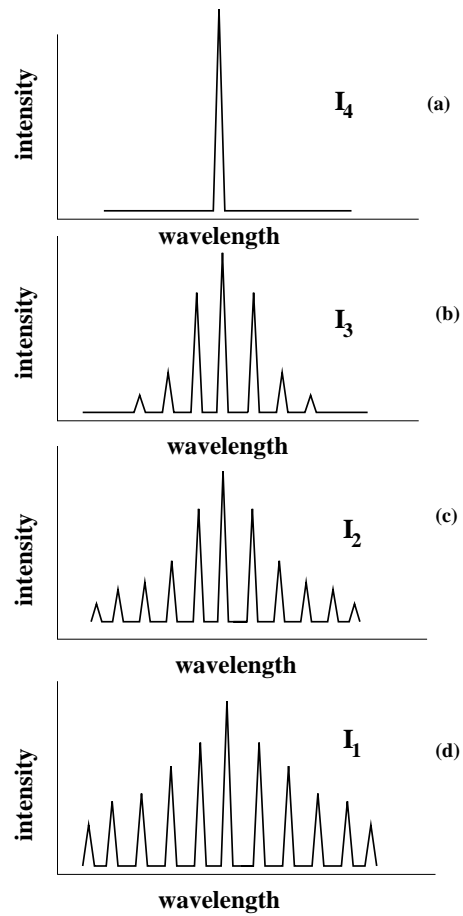


Figure 2.4: Spectra of a laser as a function of injection current. As the current increases above the threshold (figure d) to its operating current (figure a) the number of modes reduces. Current $I_1 < I_2 < I_3 < I_4$.

tuning coefficient of a diode laser is typically $0.2\text{nm}/^\circ\text{C}$, and the current tuning coefficient is $0.05\text{nm}/\text{mA}$. While the output is tunable over several nanometers by this means, there occur discontinuities or mode jumps (see figure 2.4).

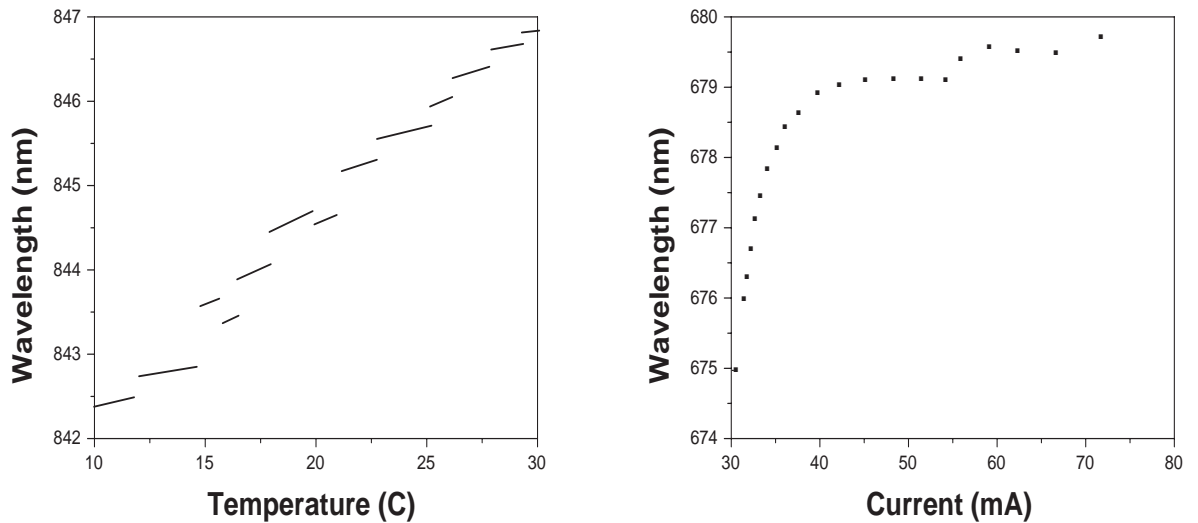


Figure 2.5: Laser diode wavelength tuning by varying the temperature of the chip (left) and injection current (right).

2.1 External Cavity Diode Laser

Laser cooling of atoms demands selective excitation of certain hyperfine transitions, which are separated by a few tens of MHz. This requires lasers with single mode output and linewidths less than the linewidth of the transition (~ few MHz). The laser should be tunable to access any transition of the hyperfine spectrum. To meet these requirements an External Cavity Diode Laser (ECDL) system is used, where an externally placed grating provides wavelength selective feedback to the laser. The lasing cavity is now determined by the back facet of the diode and the grating (figure 2.6). The increased cavity length (~ few cm) reduces intermode spacing. The main components of an ECDL are:

- **Base Plate:** the plate on which all components are mounted. This is made of duraluminium, which has a low thermal coefficient of expansion. Consequently changes in cavity length due to thermal drifts are minimised.
- **The Diode Laser:** We normally use Sanyo or Sharp diode, which delivers ~ 80mW power at ~ 100mA current.
- **The Collimating Lens:** as the output of the laser diode is divergent, this component is most

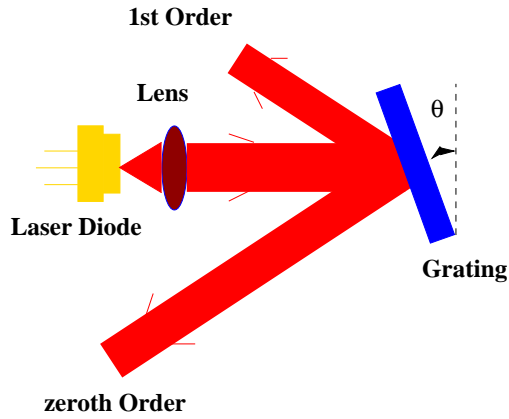


Figure 2.6: Schematic ECDL, light from the laser diode is collimated and incident on a grating at an angle θ , which splits the beam.

essential. Typically, anti-reflection coated lenses, 4-6 mm focal length are used.

- The Diffraction Grating - we usually use the grating of groove density 1200 lines/mm.

The diode laser is firmly mounted on a specially made mount that permits proper positioning of the diode, and provides a thermal mass for heat dissipation. The diode is mounted with the long axis of its elliptical output beam horizontal. The diode laser in its mount is fixed firmly to the base plate, and it is ensured that the beam propagates horizontally. Since the external cavity is extremely sensitive to vibrations and these cause mode jumps, special care was taken to prevent such vibrations. Next the lens is mounted and adjusted to obtain an elliptic beam that propagates horizontally and remains collimated over at least $\approx 10\text{m}$. The grating is fixed on a mirror mount with its grooves vertical. Usually, a blazed grating is used (figure 2.7), where the 1st order diffraction is maximised. The mirror mount permits fine adjustment of the grating by rotations about two perpendicular axes, one horizontal, one vertical. The grating mount is now fixed to the base plate such that the collimated beam from the laser falls on the grating. This results in predominantly three orders in the diffraction 0^{th} (specular reflection), $+1^{\text{st}}$, -1^{st} . The grating angle is so adjusted that the $+1^{\text{st}}$ order reflection goes back, through the lens, onto the diode, providing a feedback (figure 2.8). This is called the Littrow configuration, and the angle is obtained using the condition of maximum

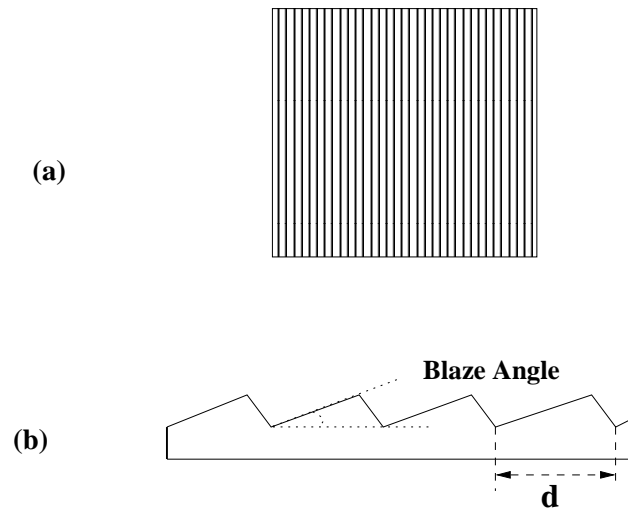


Figure 2.7: (a) Grating (b) Blaze angle on grating

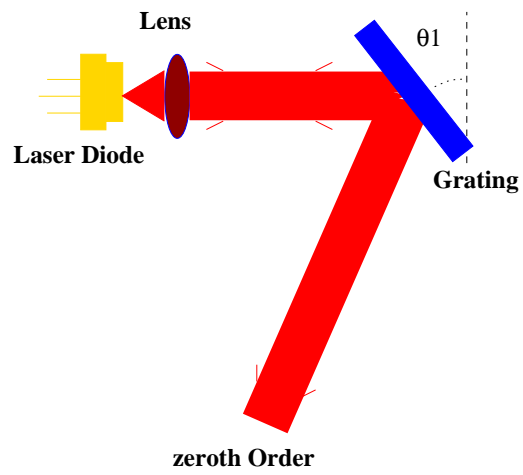


Figure 2.8: Littrow ECDL, the first order is feedback to the laser. The zeroth order is taken as output.

intensity in the m^{th} order

$$d \cdot (\sin \iota - \sin \theta) = m\lambda \quad (2.2)$$

where d is the grating constant, ι the angle of incidence of the beam on the grating and θ the angle of diffraction. θ is taken to be positive if the reflected ray lies on the other side of the normal relative to the incident ray and θ is negative if the reflected ray lies on the same side of the normal as the incident ray. In the "Littrow" configuration, the first order ($m=1$) reflection is made to be incident back onto the laser and hence $\theta = -\iota$, therefore we have

$$2d \cdot \sin \iota = \lambda \quad (2.3)$$

The angle of incidence for a given wavelength for which $\theta = \iota$, is known as the Littrow angle.

In our case (for $\lambda = 780\text{nm}$) the Littrow angle is $\sim 33^\circ$. The setting of the grating for feedback is the most crucial part in building the ECDL. Incorrect placement will not give tuning, or may result in mode jumps or multimode operation. One may slightly misalign the grating, and at low operating powers, adjust the grating while viewing the various diffraction spots using an infrared viewer to such a position that the 1st order goes back into the laser. Alternatively, the threshold current for lasing is observed for various positions of the grating. When feedback is the best, the threshold current is the least.

Once proper feedback is obtained, the output wavelength is monitored using a monochromator. We could tune our laser over nearly 4nm with no mode hop discernible on the monochromator (resolution 0.03nm).

The light from the laser diode has a certain bandwidth, i.e. a spread of wavelengths. These are dispersed upon being incident on the grating. Thus the grating selects only a narrow wavelength range $\Delta\lambda_G$ as the feedback into the laser which falls within a particular laser cavity mode and gets amplified. The rotation of the grating not only changes the angle θ (the feedback), but also the cavity length (free spectral range of the cavity). When both shifts are synchronous, frequency tuning becomes continuous over a long range of about 5

to 10nm. In most ECDL configurations, this synchronous state exists for a limited range of grating rotation angle θ . Thereafter mode hop takes place. Due to the extended cavity length the photon life-time inside the cavity becomes more and therefore, the line-width becomes less than one MHz. Line-width also depends upon the “grating constant” (typically $\sim 1\text{mm}/1200$), as this decides the band-width in the feedback. The 0^{th} order beam forms the output. However, it is evident that if the laser is tuned by means of turning the grating, the 0^{th} order beam will move correspondingly. To obtain a stationary beam, we use a beamsplitter as shown in the figure 2.9.

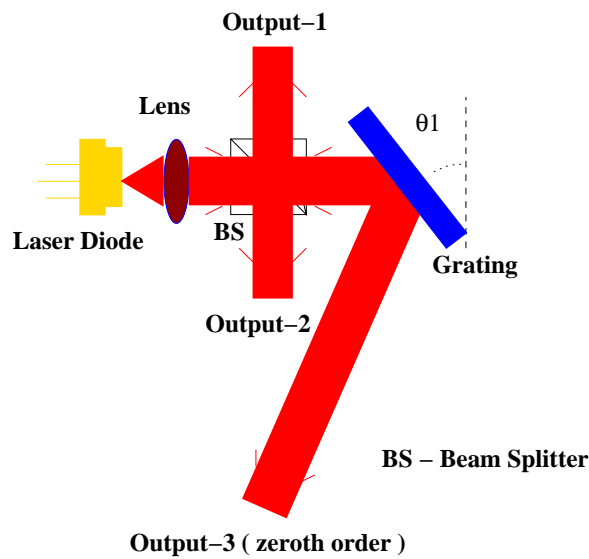


Figure 2.9: ECDL in Littrow configuration. A beam splitter has been introduced. Output-2 does not change in direction as the grating is turned.

The baseplate, with all the mounted components, is enclosed in a PVC box, to prevent the fluctuations of the ambient from affecting the performance of the laser. The baseplate is maintained at a constant temperature of about 2°C below room temperature, with the variations in temperature less than 10mK. Temperature control is essential, since laser wavelength depends upon the temperature. Changes in temperature may also alter the cavity length, resulting in a change of wavelength. Temperature control was achieved by means of a home-built PID (proportional integrator differentiator) controller, the details of which

are given in section 2.2. A thermoelectric device (Peltier) was fixed on the underside of the baseplate, and a temperature sensor near the diode. Depending on whether the temperature had deviated above or below the set temperature, the control circuit sends a current in one direction, or the opposite through the Peltier, which resulted in cooling or heating, serving to bring back the temperature to the set value.

We have built several ECDLs for our experiments at various stages of this thesis work ¹. Figures 2.10 and 2.12 show ECDLs built according to the design from reference [2]. In these ECDLs the grating is mounted on a mirror mount which has two adjustable screws to turn the grating along horizontal and a vertical axis. Figure 2.18 shows an ECDL built adopting some features from reference [3]. In this ECDL the screw for turning the grating about the vertical axis is in the mirror mount. Rotation of the grating about the horizontal axis is achieved through a screw mounted on the base plate. Various components of the ECDL are shown in figures 2.14 to 2.20 and their assembly is shown in figure 2.21.

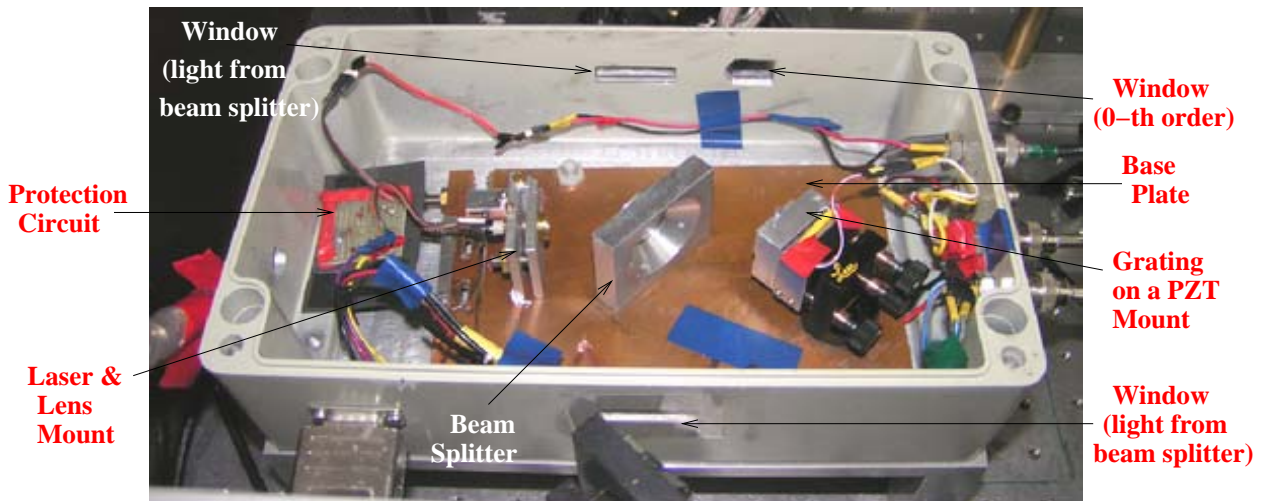


Figure 2.10: ECDL used as cooling laser

¹We are grateful to Prof. Anders Kastberg, Sweden, for giving us the basic design of temperature control and current control circuits and also several components of the cooling laser. We have subsequently modified the circuits for our specific requirements.

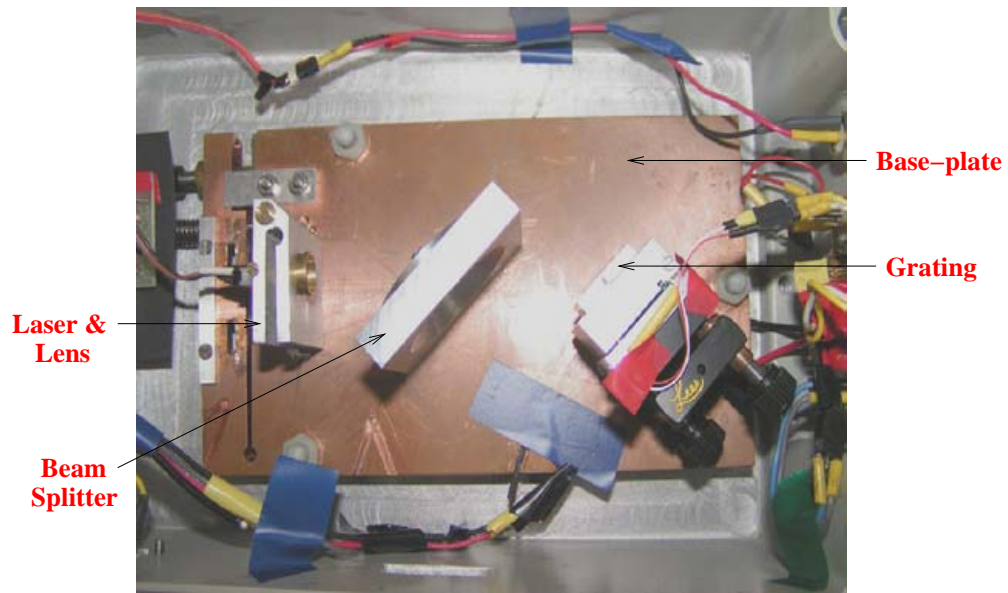


Figure 2.11: A close up view of the ECDL shown in fig 2.10

In this ECDL the screw for turning the grating about the vertical axis is in the mirror mount. Rotation of the grating about the horizontal axis is achieved through a screw mounted on the base plate. Various components of the ECDL are shown in figures 2.14 to 2.20 and their assembly is shown in figure 2.21.

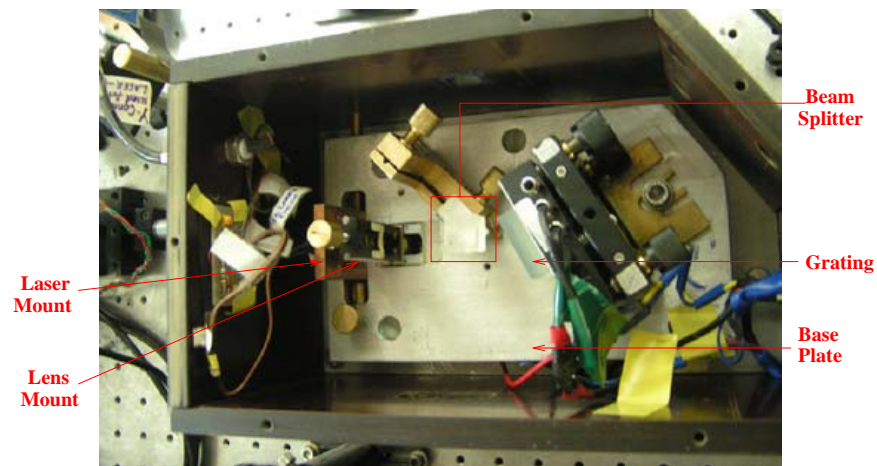


Figure 2.12: ECDL built at RRI

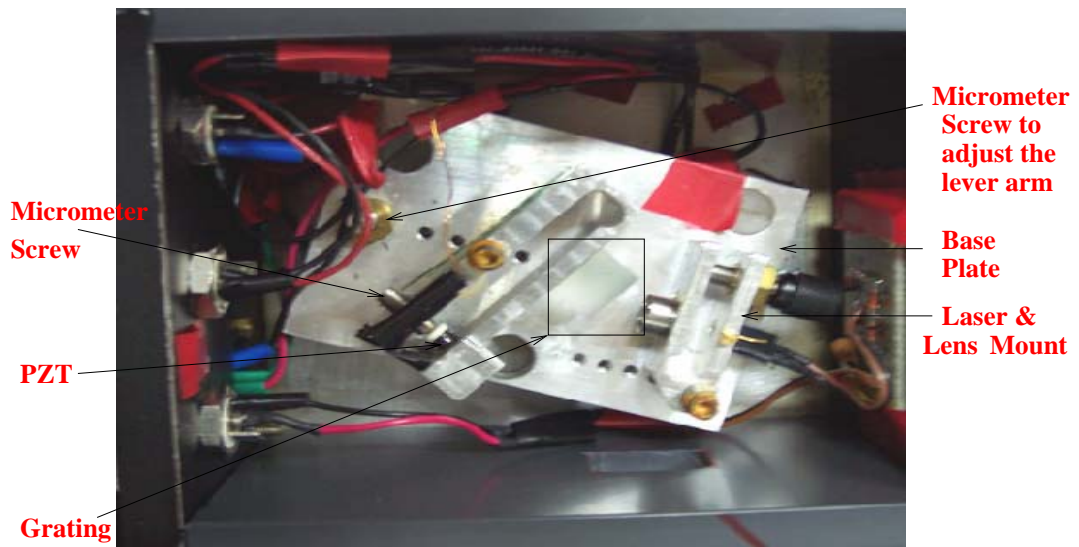


Figure 2.13: ECDL built at RRI.

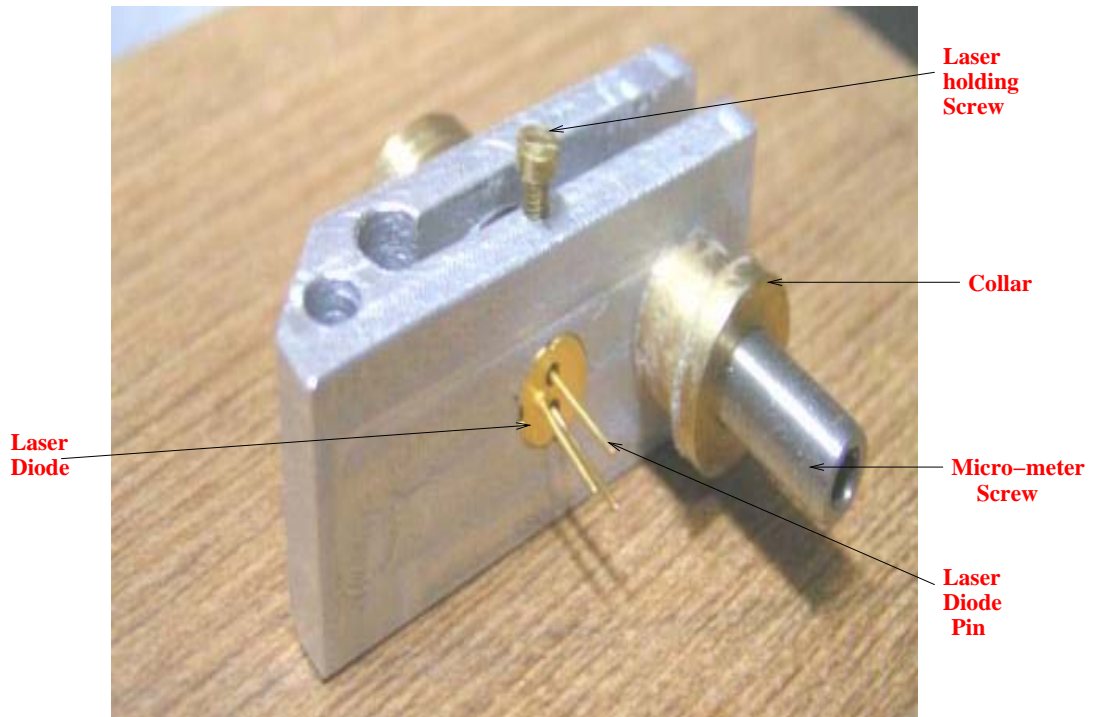


Figure 2.14: Laser-lens module back view.



Figure 2.15: Laser-lens module front view

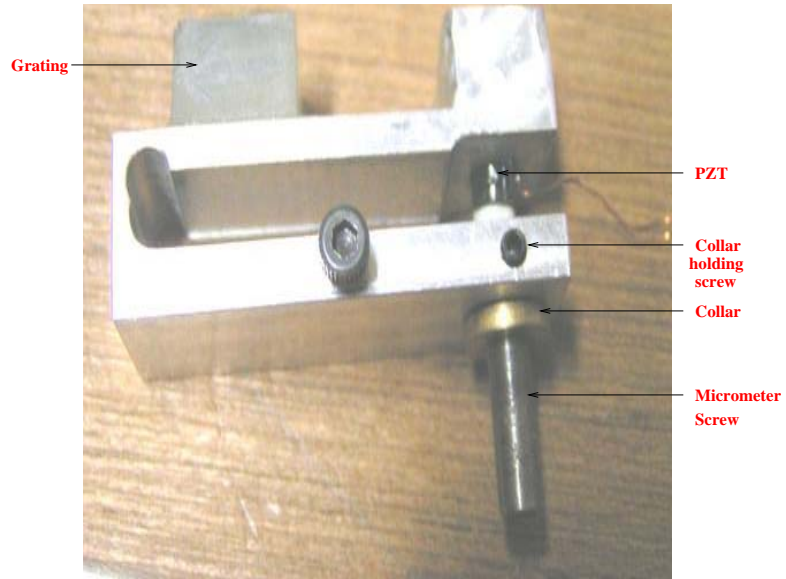
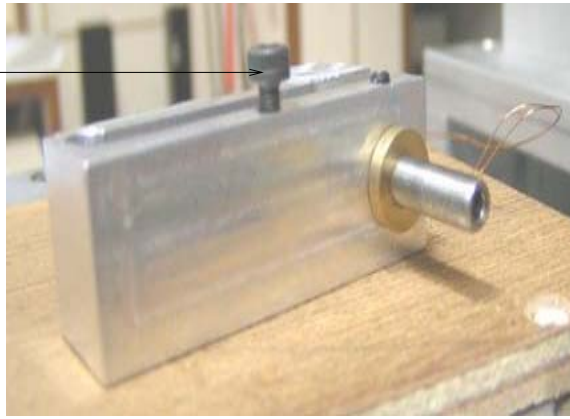


Figure 2.16: Grating mount top view.

Mount
Fixing
Screw



i

Figure 2.17: Grating mount back view.

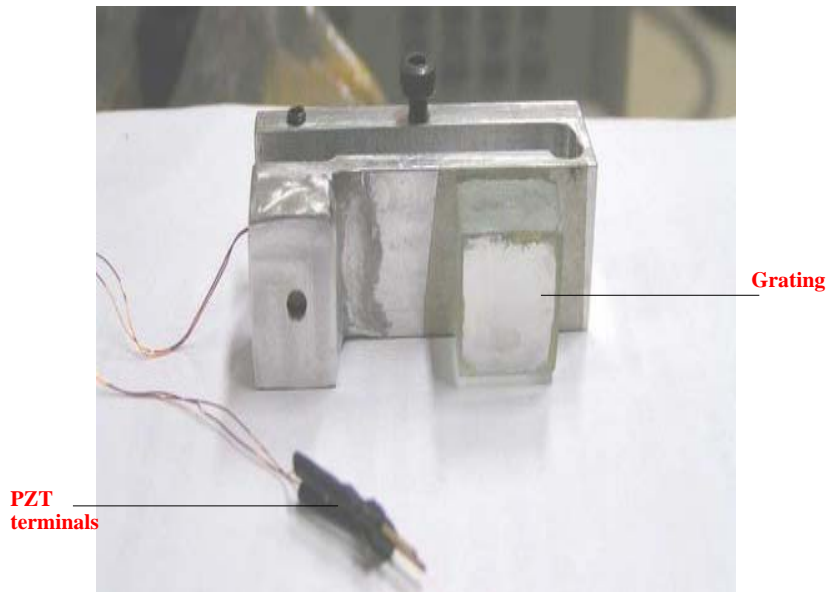


Figure 2.18: Grating mount front view.

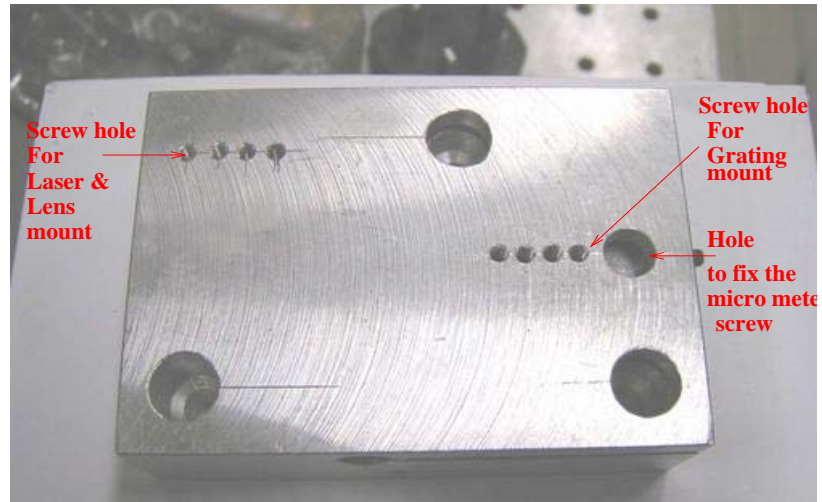


Figure 2.19: Baseplate top view.



Figure 2.20: Baseplate side view

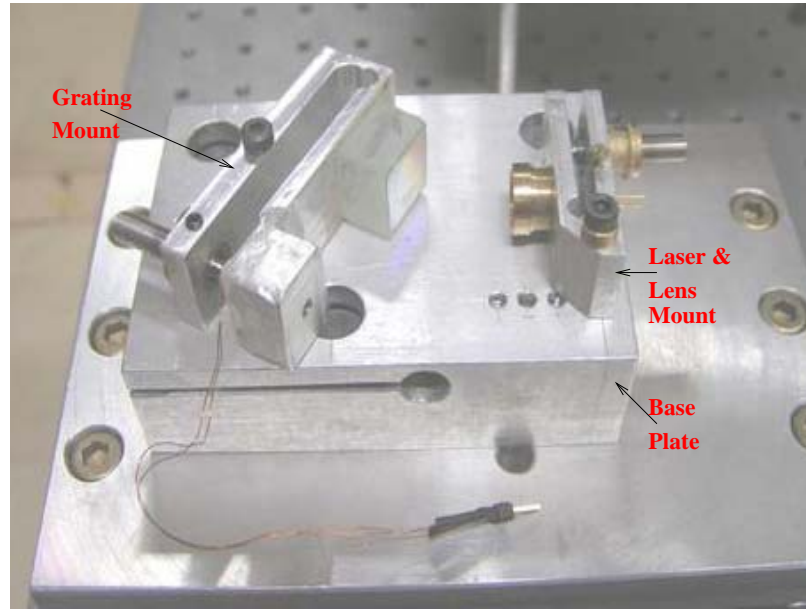


Figure 2.21: Assembled ECDL

The mode hop can be eliminated using the method described below. This was proposed by Patrick et al. [4]. In an ECDL the 1st order(plane wave) accumulates phase in two different ways, the first due to the diffraction of the plane wave at the grating surface and the second due to the propagation of the wave inside the cavity. If we consider the incident and diffracted wavefronts only which are intersecting on the grating at the point P (Figure 2.22), the electric fields on the diffracted wavefront E_d^m in the m^{th} order is related to the incident electric field E_i by the formula

$$E_d^m = E_i G_m(P) \quad (2.4)$$

Here $G_m(P)$ is the m_{th} order coefficient in the Fourier series expansion of the grating reflectance function $G(u)$ which can be written as

$$G(u) = \sum_m G_m(P) \exp(-igm) \quad (2.5)$$

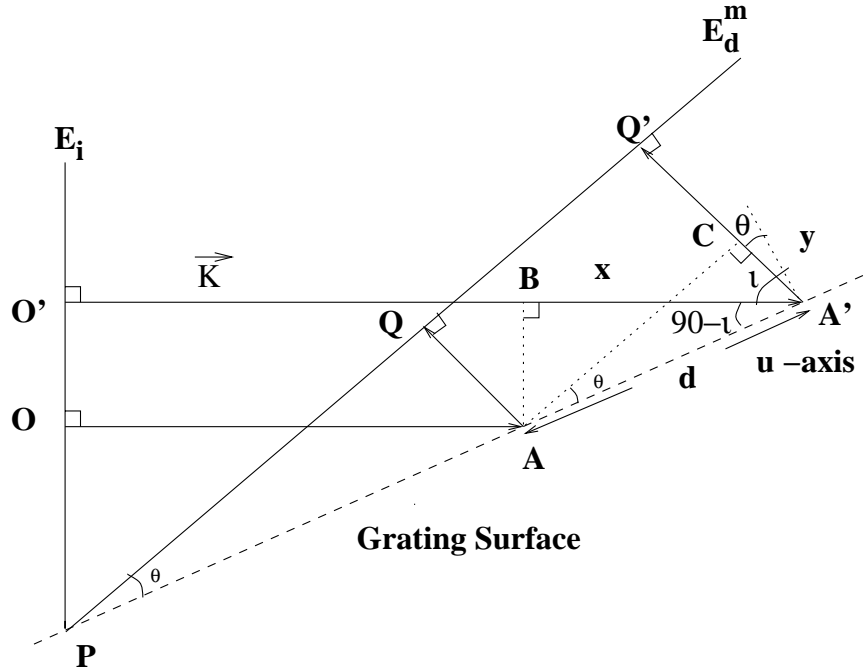


Figure 2.22: Geometry to understand the relative phase of diffracted wave

with m being zero or all positive or negative integers, and $g = 2\pi/d$.

u axis is along the surface of the grating perpendicular to the rulings, and its origin is at P .

The phase factor accumulation in the plane wave (laser beam) inside the cavity in a round trip is

$$\psi = 2k(x_0 + x_1 \cos \phi) \quad (2.6)$$

where the angle ϕ , x_0 , x_1 are as defined in the figure 2.23. As the phase ψ is a function of ϕ , it varies with the scan and the cavity does not satisfy the standing wave condition when the wavelength is scanned. This results in mode jump and the lasing shifts to the closest wavelength which satisfies the standing wave condition. It may be seen from equation 2.6 that if the extrapolated plane of the diode and the extrapolated plane of the grating intersect in a line through P , $x_0 = x_1 = 0$ and then $\psi = 0$.

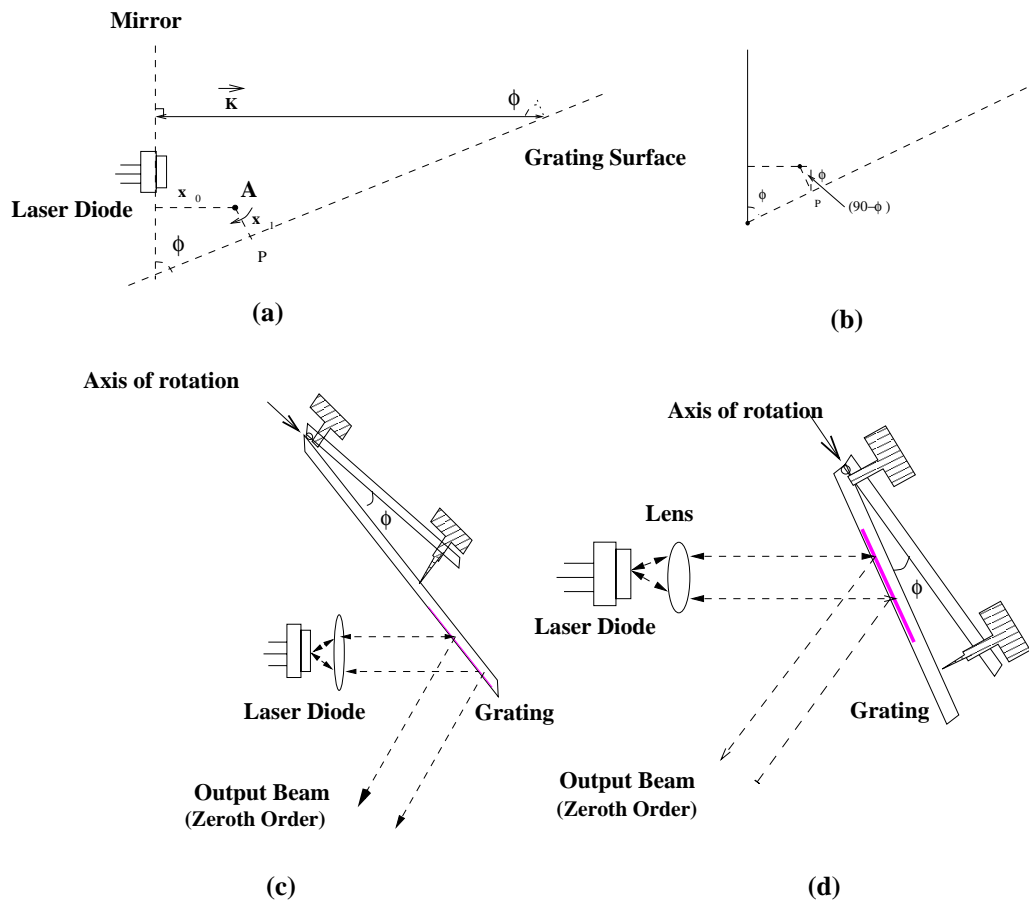


Figure 2.23: (a) and (b) geometry to understand the phase accumulation in the diffracted wave due to the propagation inside the cavity. The schematic of the synchronous oscillator (c) and Littrow cavity(d).

So the round trip phase accumulation is a constant and independent of ϕ and hence, of the feedback wavelength. This configuration of pivot is called synchronous feedback cavity mode scanning, since the returned wave maintains a constant phase relative to the incident wave throughout a scan and a “mode hop” free tuning over nearly 20nm may be achieved. We have built a “synchronous laser” whose picture is shown in figure 2.24. The grating mount has been modified, so that the pivot falls on the line extrapolated from the back facet of the diode.

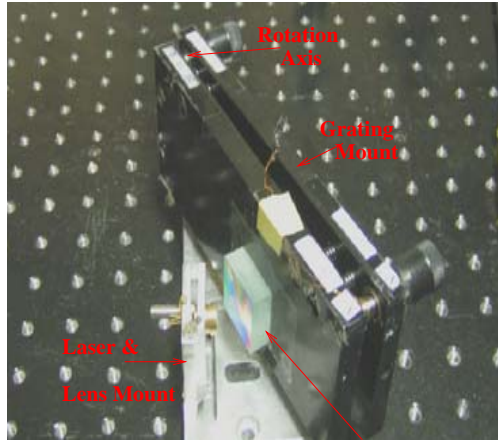


Figure 2.24: A synchronous ECDL.

2.2 Temperature stabilization of the laser diode

The block diagram of the Temperature Controller is shown in figure 2.25a. The first part of the circuit is a Wheatstone bridge (see figure 2.25b) which contains four resistors: (i) the NTC thermistor (ii) 13.3 k Ω resistor (iii) R34 and part of PT8 and (iv) R31 and part of PT8. R34 is a fixed resistance, PT8 is a potentiometer, R31 is a resistance whose value is chosen depending upon the range of the cooling required. The temperature of the base plate determines the value of the NTC resistance.

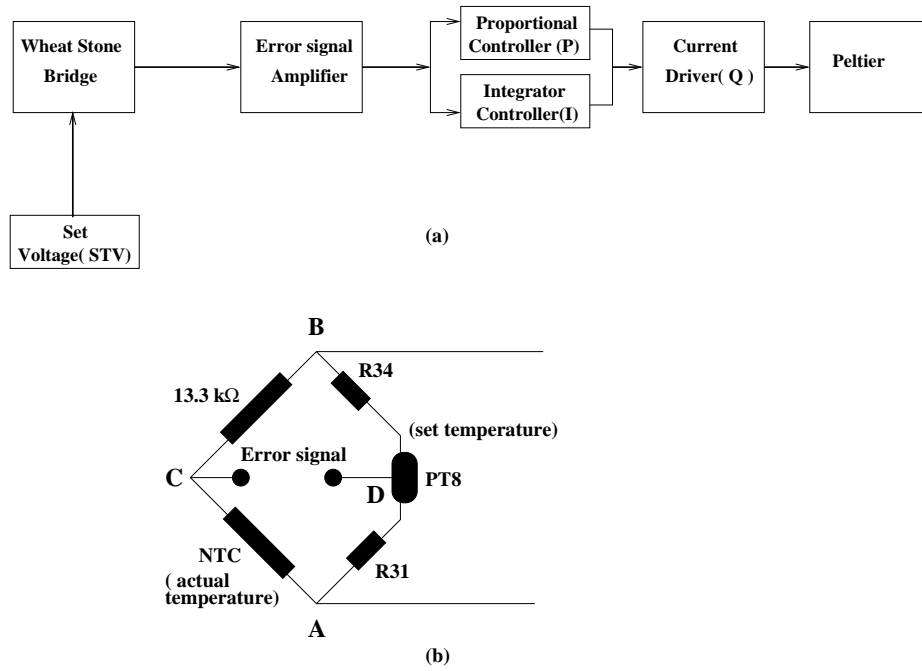


Figure 2.25: (a) block diagram of the temperature controller (b) the details of the Wheatstone Bridge.

A constant voltage source is connected between the nodes A and B. The potentiometer PT8 is set at a value which determines the temperature at which the bridge will be balanced. When the actual temperature T_{actual} of the baseplate differs from the set value T_{set} the bridge is out of balance and a voltage V_{ob} appears across C and D. The sign of this voltage depends on whether T_{actual} is more than T_{set} or less than T_{set} . V_{ob} is fed to a Proportional and Integrator (PI) controller stage. The PI applies power

$$W = p(V_{ob}) + \alpha \int_t^{t+\tau} V_{ob} dt \quad (2.7)$$

to the Peltier, where p is the proportional gain of the controller. α the integration constant. The effect of the integral term is to change the Peltier power until the time averaged value of V_{ob} becomes zero. We use MOSFETs 2SK1058(PMOS) and 2SJ162(NMOS) as current drivers for driving the Peltier. The PI controller decides the direction and the amount of the current to be sent to the Peltier to achieve the required cooling or heating of the baseplate.

Typically, when $T_{actual} - T_{set}$ corresponds to $\sim 2^{\circ}\text{C}$, V_{ob} amounts to 4V. Initially only the proportional stage is switched on, and when V_{ob} reduces to $\approx 2\text{V}$ the integrator stage is also switched on, which integrates V_{ob} over a certain time. The integrator stage ensures V_{ob} reaches zero rapidly, and therefore T_{act} becomes equal to T_{set} . The temperature controller stabilises the laser temperature to about $\pm 10\text{mK}$ of its set value within 30 minutes.

2.3 Laser diode protection circuit

The laser diode is operated in constant current mode. To obtain a steady output wavelength, we have built a laser driver using constant current driver LD1255 (by Thorlabs), capable of giving upto 150mA, stable to $1\mu\text{A}$. It is run from a rechargeable battery of 12V. This is because laser diodes are very sensitive to voltage spikes. The active region is very narrow ($3\mu\text{m}$) and an overvoltage of just a volt will result in extremely large electric fields. We also use a protection circuit, placed very close to the laser diode (figures 2.10). The purpose of this circuit is

1. to protect laser from over voltage or spikes
2. to protect the laser from reverse voltage
3. to maintain steady current if there is a momentary reduction in voltage.
4. to limit the current through the laser diode, even if current driver is set to send more.

As the pin configurations and the characteristic parameters are different for different laser diodes, separate protection circuits have to be built specially for each laser diode.

Each laser diode package contains a laser diode and a photo diode that may be used to monitor the output power of the laser. The laser diode and the photo diode have one common electrode connected to the package body. So each laser diode package has three electrodes, one common electrode and two free electrodes one from the laser diode and the other one from the photo diode inside. Therefore, according to the electrode configurations

the laser diodes can be divided into two major categories, namely body “common anode” and “common cathode” (figure 2.26).

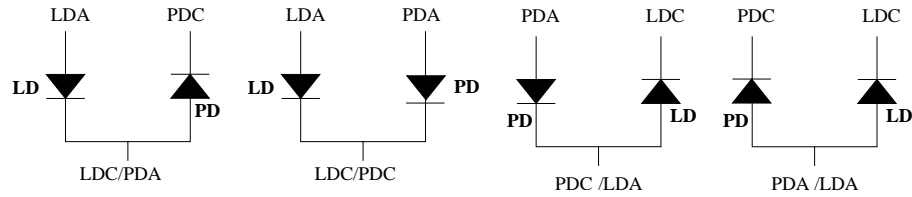


Figure 2.26: Possible pin configuration of diode lasers

Figure 2.27a shows how a protection circuit is used with a laser diode. The protection circuits for the two types of laser diodes are shown in figures 2.27b, and 2.27c. The circuit takes power from LD1255 through terminals LD+ and LD-, the current flows through the resistance (R) and then can split into four parallel arms. One of the arms contains the laser diode which is forward biased, another contains the three forward biased fast diodes in series. Another arm contains a reverse biased fast diode and the last arm has a capacitor (~ 100nF).

Under normal operation, a steady current flows through the laser diode and no current flows through the other three arms.

The value of the resistance of the laser diode R_D is calculated from the data V_{op} and I_{max}

$$R_D = \frac{V_{op}}{I_{max}}. \quad (2.8)$$

The voltage across the diode laser should be maintained at V_{op} . Therefore, the value of R has to be chosen properly. If the supply voltage between LD+ and LD- be V_{bat} , R can be calculated from the relation

$$R = \frac{V_{bat} - V_{op}}{I_{max}}. \quad (2.9)$$

The functions of the other three arms of the circuit are as follows- if there is an over voltage the diodes in series come into conduction and ensure that no excess current flows through the laser diode. The number of fast diodes n is chosen such that n is the smallest number for

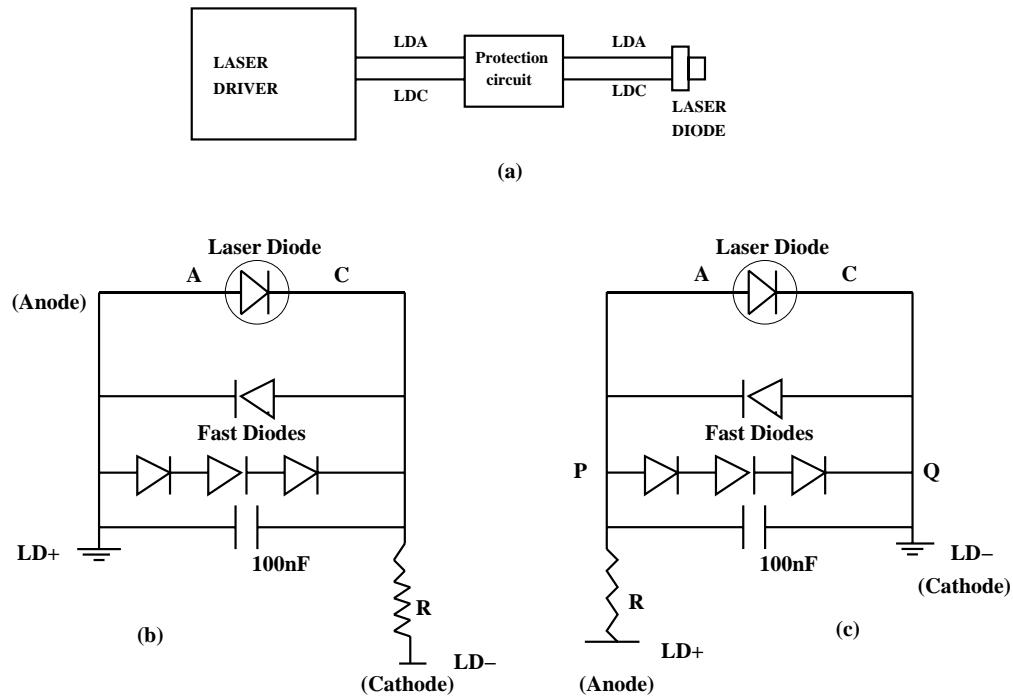


Figure 2.27: (a) shows how the protection circuit is used for a laser diode (b) protection circuit for common anode laser diode (c) protection circuit for common cathode laser diode

which $(n \times 0.7) \geq V_{op}$. Here, 0.7 V is the voltage across the diodes when they are conducting. Thus under normal operation no current flows through the n fast diodes in series, as the voltage V_{PQ} across them = V_{op} , the voltage across the laser diode in conduction. However, when a spike or over voltage occurs, V_{PQ} exceeds V_{op} , and also $(n \times 0.7)$ Volts. The fast diodes now start conducting, providing a low resistance path to the current, and thus protecting the laser diode. If the protection circuit gets connected to laser driver wrongly (LDA and LDC get exchanged) then only the reverse biased diode will conduct. When the voltage suddenly drops, the capacitor acts as a source, maintaining the laser current.

For example if $V_{bat} = 12$ Volts, $V_{op} = 2$ volts, $I_{max} = 120$ mA, the minimum value of R becomes 83.5Ω . In this case n , the number of fast diodes to be connected is 3.

2.4 The saturation absorption set-up

In spite of the passive stability of the laser diode injection current and the active stabilization of temperature, drifts in frequency of a few tens of MHz can occur over a period of few minutes. Mechanical vibrations too can cause changes in the laser wavelength. Thus some form of active stabilization of the frequency of the laser is required. This requires a frequency reference, which is obtained by using Doppler free saturated absorption spectroscopy signal of Rb atoms. This is described below.

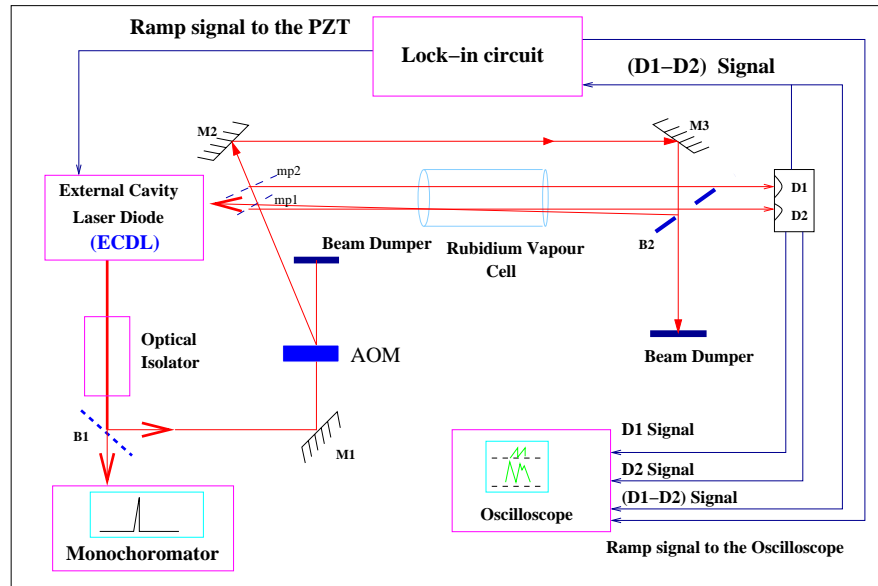


Figure 2.28: Doppler free saturated absorption spectroscopy set-up; M's are mirrors B's are beam splitters and mp's are microscope slides, AOM acousto-optic-modulator, D's are photo detectors.

The Doppler width for a gas can be estimated from $\Delta\nu = 2kv_{mp}$, where v_{mp} = most probable velocity at the temperature of the gas, and $k = 2\pi/\lambda$. At room temperature both for ^{85}Rb and ^{87}Rb $v_{mp} \approx 230\text{m/s}$ and the Doppler width is $\approx 2\text{GHz}$. The natural line width

of a hyperfine transition on the other hand , $\sim 2\pi \times 6\text{MHz}$, and the spacing between various hyperfine levels are few tens to few hundreds of MHz. These, therefore, can not be resolved as the Doppler line-width is much larger. The technique of Doppler free saturation absorption is used to select out, from a collection of atoms moving with Maxwellian distribution of velocities, those atoms that have zero velocity component in the direction of the input beam. This then yields absorption lines, which have widths equalling their natural linewidth.

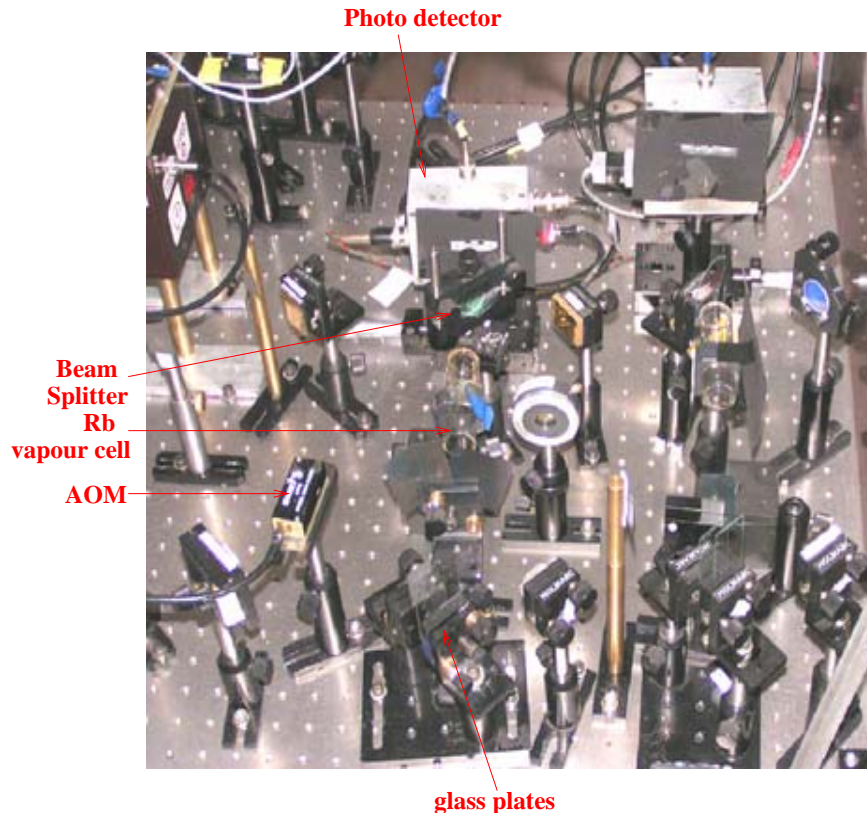


Figure 2.29: A picture of the saturated absorption spectroscopy set-up from our laboratory

The typical Doppler-free saturated absorption set-up is shown in figure 2.28, and a photograph of the same from our laboratory is shown in figure 2.29. Two mutually parallel microscope glass plates(mp) placed at 45° to the main laser beam reflect a small fraction ($\approx 4\%$ of the incident intensity) of the laser light so that we get two

parallel weak beams (called probe and reference). These two beams pass through the Rb vapour cell and fall onto two identical photo detectors which are connected with the required circuitry. If the laser frequency is scanned across one set of hyperfine transitions and the two photo detector outputs are monitored in the oscilloscope both outputs from the probe and the reference show identical Doppler-broadened spectra as shown in figure 2.30.

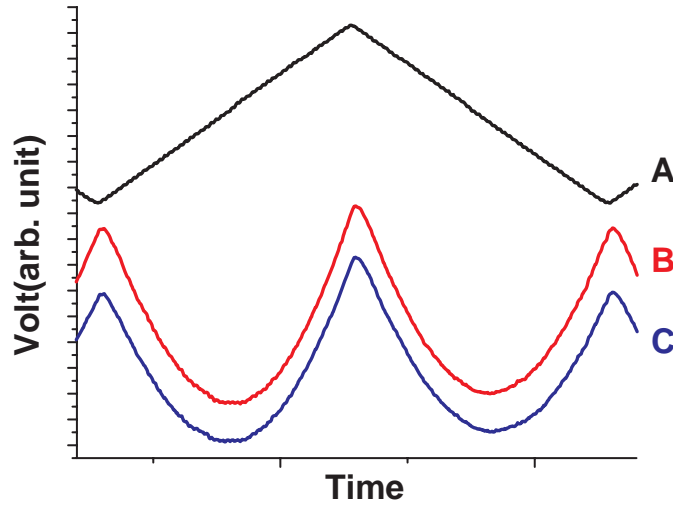


Figure 2.30: Oscilloscope trace of A: ramp voltage to piezo, B,C: Doppler transmission profiles through vapour cell of probe and reference beams.

The high intensity part of the main laser beam which gets refracted through the microscope slides (mp's) is reflected by two mirrors and is aligned to counter-propagate with the probe beam inside the *Rb* vapour cell. This forms the saturating or pump beam.

For an atom moving with a non-zero velocity along the beam axis the Doppler shifts of the probe and pump beams are different as the atom is moving in opposite direction relative to the two beams and the Doppler shifts of the two are equal but opposite. So, as the laser frequency is changed either the probe or pump beam comes into resonance.

Only for atoms with $v=0$, the pump and probe beams simultaneously come into resonance. The absorption of the probe beam is diminished by the strong pump beam. This

results in a narrow dip at the three hyperfine transition frequencies (figure 2.31). In addition an atom can have such a velocity v such that the Doppler shifted probe beam is in resonance with a hyperfine transition ω_i while the Doppler shifted pump beam is in resonance with another hyperfine transition ω_j . This will happen when $\omega_L = (\omega_i + \omega_j)/2$. Therefore, three more dips will be seen, and in all, six dips will be seen in each scan.

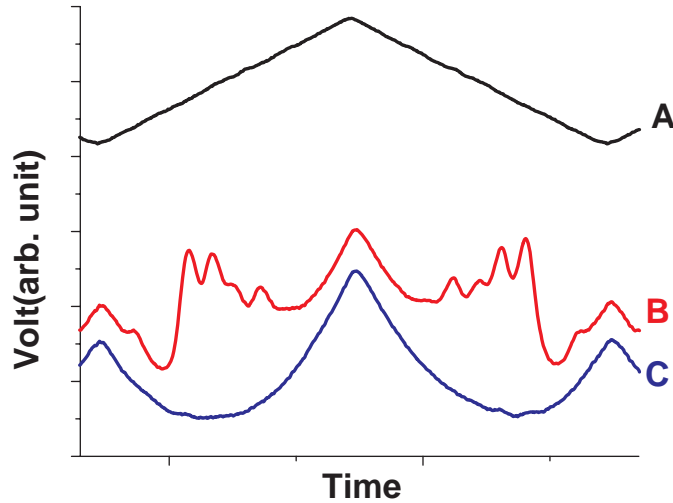


Figure 2.31: Oscilloscope traces of A. ramp to piezo, B. Transmission of probe with a strong counter-propagating pump. C. Transmission of reference beam. Due to saturation of absorption, the hyperfine transitions can be resolved in the probe transmission.

To get the best hyperfine spectrum (well resolved peaks) laser should have an extremely narrow line-width (~ 1 MHz), and the overlapping of the probe and the pump beams should be maximum inside the tube. The overlapping would be best if they cross each other at an angle ≤ 10 mradian. In our saturated absorption set-up the probe and pump beams are aligned collinear, and counter-propagating, so that they overlap over the complete length of the tube.

We take difference in absorption of probe and reference beam so as to obtain narrow peaks (figure 2.32) over a flat background. The triplet hyperfine transition frequencies ω_1 ,

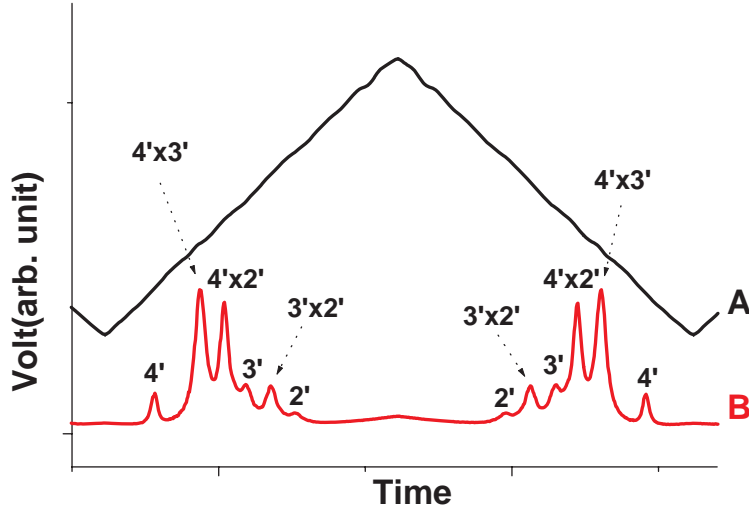


Figure 2.32: Oscilloscope trace of A. Voltage ramp to piezo and B. the difference of probe and reference signals, which gives a flat background. Shown is the $F = 3- \rightarrow F'$ transitions for ^{85}Rb . Cross over peaks are labelled as $i' \times j'$.

ω_2 , ω_3 and the crossover frequencies $\frac{\omega_1+\omega_2}{2}$, $\frac{\omega_1+\omega_3}{2}$, $\frac{\omega_2+\omega_3}{2}$ are well resolved. The crossover peaks have a line-width slightly larger than the natural line-width.

2.5 Laser frequency locking

We next describe the home-built “lock-in” circuit which uses a servo-controlled feedback loop to hold the laser frequency constant.

A Doppler free saturated absorption spectroscopy set-up is used to monitor the instantaneous frequency of the laser by looking at the hyperfine spectrum of the atomic transition. The laser frequency is scanned across the hyperfine lines by sending a ramp signal to the piezo-electric-transducer (PZT) attached in the grating mount. The ramp signal sent to the PZT is drawn from the “lock-in”. We then reduce the ramp amplitude so that the frequency scanning gives rise to only one of the peaks (a real peak or cross-over peak) of the saturated absorption spectrum, the one to which we want to lock the laser frequency (see figure2.33a).

The ramp signal sent to the PZT is modulated by using a sinewave of frequency 1kHz. The detector output, which earlier gave a smooth peak, is now distorted due to the modulation. This new signal is multiplied in a multiplier stage in the lock-in circuit with the same sine wave which was used to modulate the ramp signal. The output of this stage is passed through a low pass filter. A dc signal is obtained which is the derivative signal of the hyperfine transition absorption. The zero of the derivative corresponds to the peak of the hyperfine absorption where we want to lock the laser frequency (see figure 2.33b - 2.33d). In mathematical

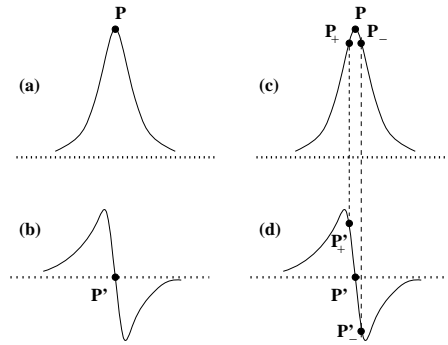


Figure 2.33: (a) atomic transition line (b) derivative of the line. (c) and (d) are to show the lock position on the peak and on the derivative signal.

terms, this may be understood as follows:

The instantaneous laser frequency is a function of the ramp voltage $V(t) = at$ to the Piezo at the time t . The corresponding saturated absorption signal $S(t) = f(V(t)) = f(at)$.

When the ramp is modulated using a sinewave $\Delta V = A \sin \omega t$, this function becomes $f(at + A \sin \omega t) = f(at + \Delta V)$. Therefore, the laser frequency becomes,

$$S = f(at + \Delta V) \quad (2.10)$$

$$= \left[f(at) + \left(\frac{df}{dV} \right)_{V=at} (\Delta V) + \frac{1}{2} \left(\frac{d^2 f}{dV^2} \right)_{V=at} (\Delta V)^2 + \dots \right] \quad (2.11)$$

$$= f(at) + \left(\frac{df}{dV} \right)_{V=at} (A \sin \omega t) + \dots \quad (2.12)$$

After the multiplication using a sinewave $A'(\sin \omega t + \phi)$ derived from the same oscillator, this becomes $S \times A' \sin(\omega t + \phi)$. This can be expanded in powers of ΔV . If ΔV is small we can retain only the first power of ΔV and neglect the higher powers. Then

$$S \times A' \sin(\omega t + \phi) = \left(f(at)A' \sin(\omega t + \phi) + \left(\frac{df}{dV} \right)_{V=at} (AA' \sin \omega t \sin(\omega t + \phi)) \right) \quad (2.13)$$

$$= \left(f(at)A' \sin(\omega t + \phi) + \left(\frac{df}{dV} \right)_{V=at} \left(\frac{AA'}{2} (\cos \phi - \cos(2\omega t + \phi)) \right) \right) \quad (2.14)$$

If this signal is passed through a low pass filter only the dc component $\left(\frac{df}{dV} \right)_{V=at} \left(\frac{AA'}{2} \right) \cos \phi$ will come out of the filter. This output is proportional to $\left(\frac{df}{dV} \right)_{V=at}$ ie it is proportional to the derivative of the saturated absorption signal. This derivative can be maximized by making $\phi = 0$ ie by locking the reference phase to the signal phase. The derivative becomes zero at the peak of the saturated absorption signal. (see figure 2.33a and b). Block diagram of a lock-in circuit is shown in figure 2.34.

To lock the laser, we switch to the manual mode, where a modulated dc signal is applied to the piezo, instead of a ramp. It is varied manually to scan over the required atomic transition peak. The derivative signal is seen on the oscilloscope and at the point of the scan when it reaches zero the “lock switch” is enabled. When the lock switch is on, any deviation of the derivative from the zero position will give an error voltage which is passed through an integrator to get an amplified signal opposite in phase to the error signal. This is fed to the Piezo which brings the frequency of the laser back to its locked value.

To apply a suitable detuning to the laser an acousto-optic-modulator is used in the laser beam path in the saturated absorption spectroscopy set-up, which shifts the laser frequency. The shifted laser frequency is locked to the derivative at the peak of the hyperfine transition.

Since the crossover peaks are taller than the true hyperfine absorption peaks, it is more convenient to use the cross-over peak $(\omega_2 + \omega_3)/2$ as reference to lock the laser. However, the detuning of the laser for laser cooling is measured from ω_3 . So the laser beam going to the saturable absorption set-up is shifted in frequency by $|(\omega_2 - \omega_3)/2|$. Thus the laser can be locked at a particular detuning δ_0 relative to the crossover peak.

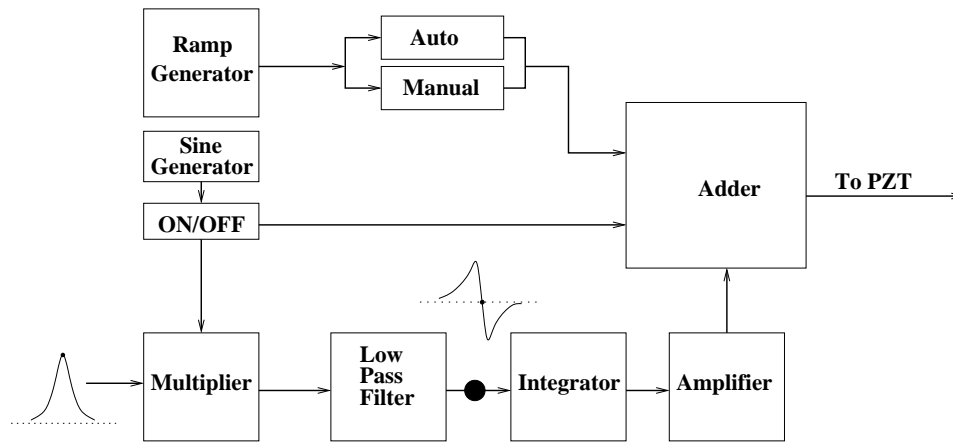


Figure 2.34: Block diagram of the lock-in circuit.

2.6 MOT chamber

The vacuum chamber used for our MOT is made of stainless steel with volume about 2 liters. It has an octagonal vertical cross-section and rectangular horizontal cross-section(see figure 2.35.). Each side of the octagon is ~ 10 cm. Width of the chamber is also about ~ 10 cm. It has a total of 14 ports. Two ports hold the feedthroughs for the Rb getter sources and the rest are the ports for optical access. The viewports connected along the sides of the octagon are of diameter 2.75 inches, the two viewports fixed on the octagonal surfaces of the chamber are of diameter 6 inches. For these ten viewports, lines drawn normally through the center intersect at the center of the chamber. There are other two view ports located exactly below the two large viewports, these are of diameter 1.33 inches. Our vacuum chamber is made by New Poona Industries, India, and we use the conflat view ports made by Varian.

For achieving good vacuum, the chamber was baked, initially by closing all ports with metal endcaps and winding heating tape over the entire chamber and connectors. The set-up was heated to 400°C , while being pumped by the turbo pump. At first, due to degassing, the pressure rose. After about 8 hours, the pressure began to fall. Baking was continued for ≈ 48 hrs, then the temperature was gradually brought to room temperature. The metal windows were then replaced with glass viewports and this time baking was confined to 200°C . During

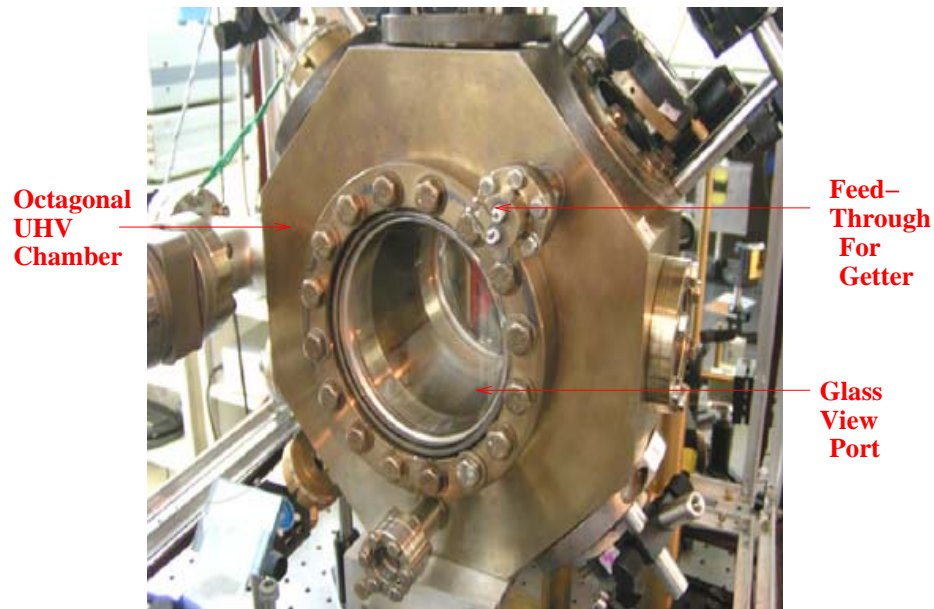


Figure 2.35: Picture of UHV chamber

baking a low current was passed through the getter to remove included gas, and the ion pump was also heated. The vacuum layout is shown in figure 2.36. We used Varian -Vacion 40Plus and Varian V70 TurboStack, and a Varian Bayard-Alpert ion gauge to measure the vacuum in the chamber.

The rubidium getter sources we use in our laboratory are from the company SAES, Italy. These getters dispense alkali atoms and are designed for use in industry. The getter is a Rb compound and a reducing agent enclosed in a stainless steel boat. The compound is stable at room temperature and, therefore, the boat can be handled easily. When a few amperes of current are passed through the boat, its temperature rises to several hundred degrees centigrade. In ultra high vacuum, the Rb is released as vapour. Since the chemical reaction between the Rb compound and reducing agent is a threshold process, no Rb vapor is released below a threshold value of the current, which is about 2.2 A.

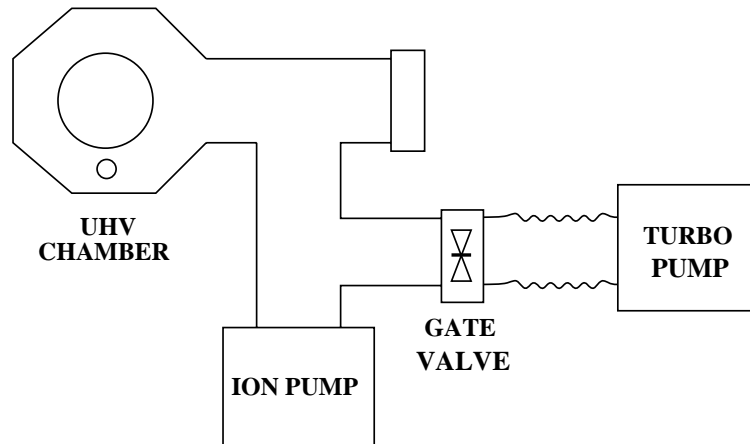


Figure 2.36: Vacuum pump lay-out.

We usually connect three stripes in series and spot weld to a feedthrough. This way we can avoid frequent replacement of the getter, which essentially needs the breaking of vacuum.

2.7 Trap coils and water jacket; compensating coils

To trap the atoms with a MOT we have two anti- Helmholtz coils placed on the two sides of the chamber parallel to the octagonal surfaces along the z axis. Diameter of each coil is ~ 9 cm, each coil has 140 turns of copper wire of gauge 18. The separation between the coils ~ 13 cm. Using these coils a quadrupolar field can be produced with a gradient of ~ 10 G/cm with zero field at the geometrical center of the chamber. The required current to be sent through the coils to obtain this field gradient is ~ 11 A. To avoid excess heating and burn out of the coils, the coils are housed in a water jacket and water is circulated in a closed path while the experiment is on.

To test the field gradient in the UHV chamber, the anti- Helmholtz coils are positioned before fixing the viewports. To obtain the required field gradient a Hall probe is inserted

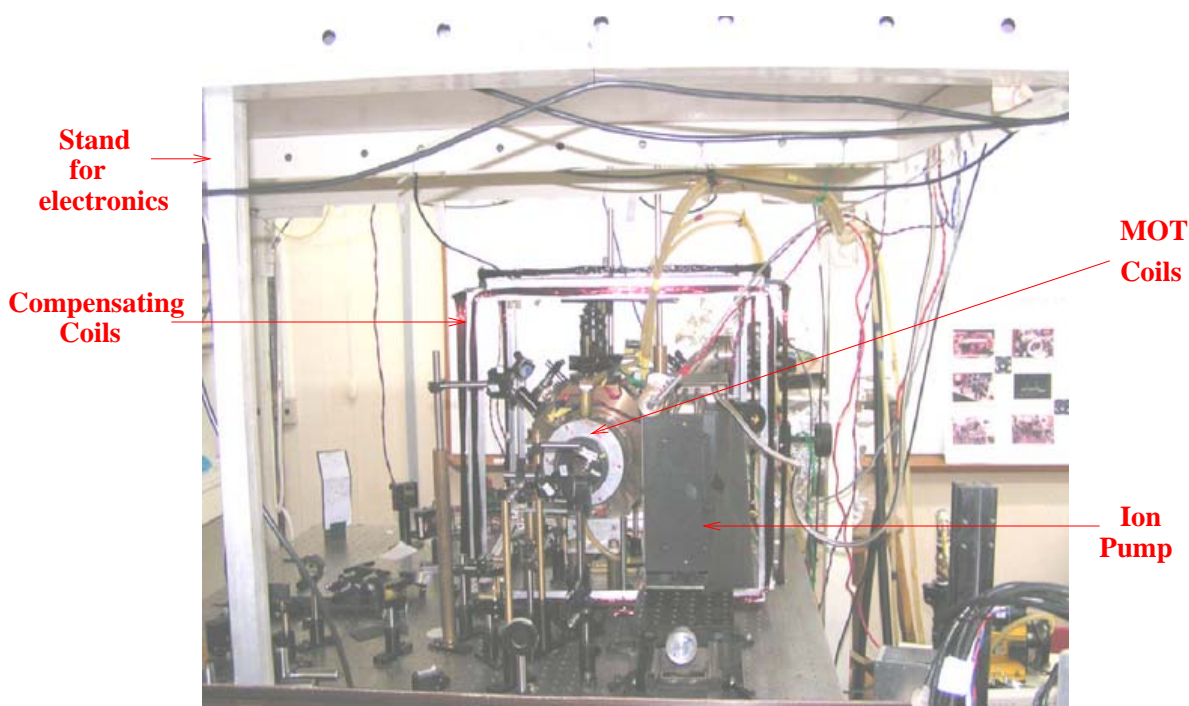


Figure 2.37: A side view of our entire MOT set-up

in the chamber, and the coils can be positioned to ensure that at the center of the chamber the field is zero. The required current to the coils is drawn from one or two current sources, and the value of the current is noted for future use. In practice we find that the magnetic field at the geometrical center of the UHV chamber is non-zero when the quadrupolar field is made zero, and this is due to the presence of the magnet in the ion pump and also due to the earth's magnetic field. To nullify these we use a set of six compensating coils(see figure 2.37) surrounding the chamber, which carry current in suitable directions.

2.8 Optical Layout and alignment

We used a vibration isolation (TMC 8'×4'×18'') table, on which the lasers and their saturated absorption setups were kept at one end. These were enclosed in a box -like chamber made of hylam sheets. This served two purposes- firstly the lasers were isolated from the fluctuations

of the ambient temperature and secondly, as the hylam sheets were opaque, switching on or off, the room lights did not affect the saturation absorption signals or the locking of the laser. The schematic of the layout is shown in figure 2.38. Figure 2.39 and 2.40 are the photographs of a part of our experimental set-up. The UHV chamber is kept at the other end of the table. It is connected to a turbo pump placed on separate stand mounted on the floor by means of a bellow. All electronics control units are kept on a stand that covers the optics table at a height of 6', and is mechanically not connected to the optics table. As the wavelength required for

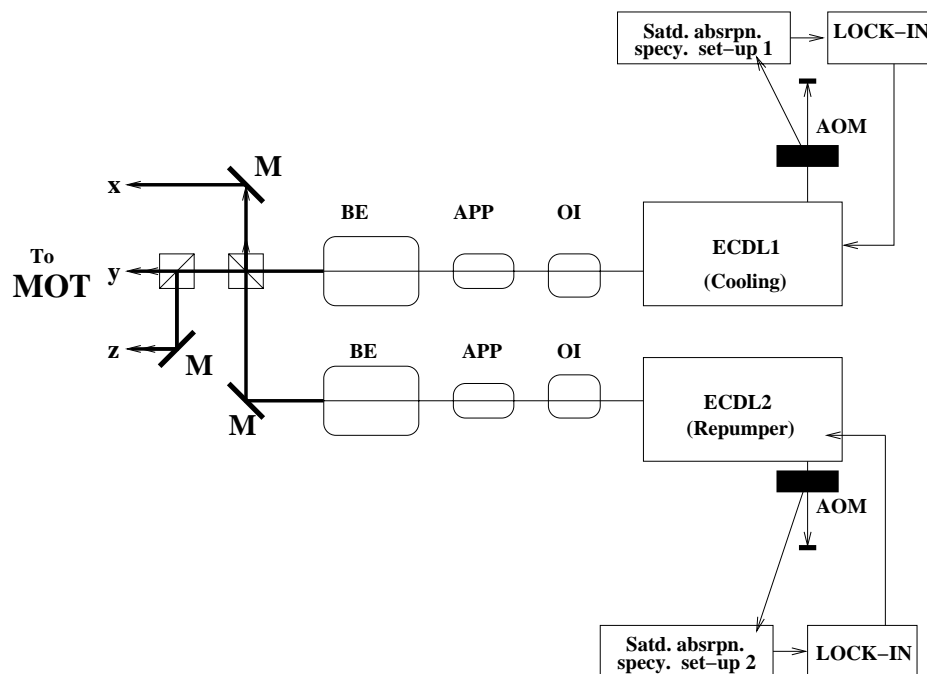


Figure 2.38: A schematic of organizing EC DLs and derivation of MOT beams in the lab. M → mirror, OI → optical isolator, APP → anamorphic prism pair, BE → beam expander, AOM → acousto-optic-modulator.

laser cooling Rb($\sim 780\text{nm}$) is in the near infrared, we use infra-red viewers or infrared cards for alignment of the beams. The beam from the cooling laser is expanded to obtain a circular beam of about 1cm diameter. The typical intensity is $1\text{mW}/\text{cm}^2$. By means of beam splitters and mirrors, this is divided into three beams, of nearly the same intensity.

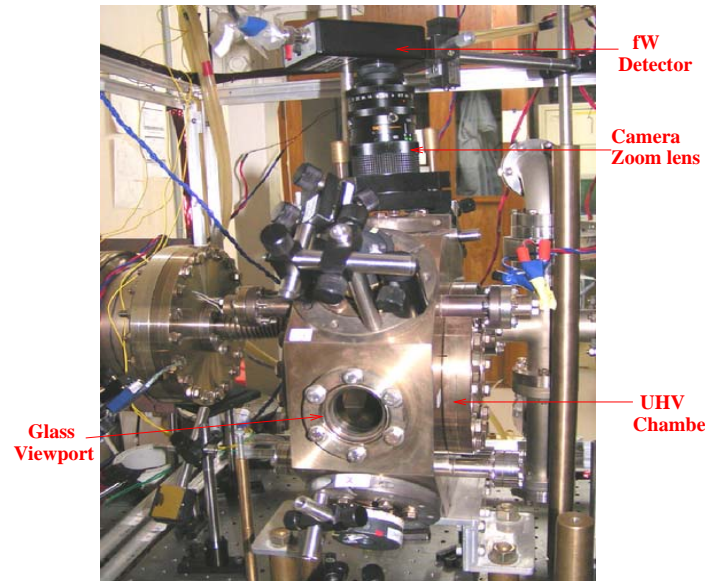


Figure 2.39: Picture of a part of the MOT set-up

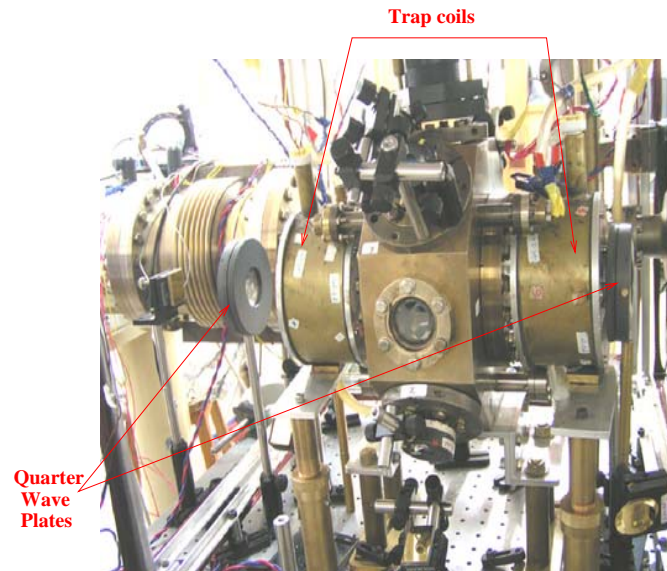


Figure 2.40: Picture of a part of the MOT set-up

Using quarter-wave-plates, two of the beams are made σ^+ polarized and one beam (along the z axis) σ^- polarized . These then enter the chamber from the +x, +y and +z directions. They exit from the diametrically opposite windows of the chamber, pass through quarter wave plates and are retro-reflected back into the chamber, now with opposite helicity.

It is essential that all six beams intersect at the centre of the chamber, and that the zero of the quadrupolar field due to the MOT coils coincides with this point of intersection. For this purpose we introduce Rb into the chamber, and view the fluorescence. The beams appear as straight tracks, as the atoms in the path of the beams scatter the resonant light. The beams are viewed from two non-equivalent angles using a CCD camera. The back reflected beams are brought into coincidence with the on-coming beam by fine adjustment of the mirrors. We reduce the diameter of the beams to a few mm to check that the overlap of the laser beams is perfect. The beams are aligned to intersect exactly at the center of the chamber. The beam from the repumper is also split into three, and it follows an identical path as the cooling beams. Once the cooling and repumper beams are aligned, the cooling and repumper lasers are locked to the relevant transitions. When the current through the magnetic coils is switched on a cloud forms almost instantaneously, and appears as bright patch when viewed by the CCD camera (see figure 2.41). In the process of development of our MOT we have referred to the articles [2], [5] and the references therein.

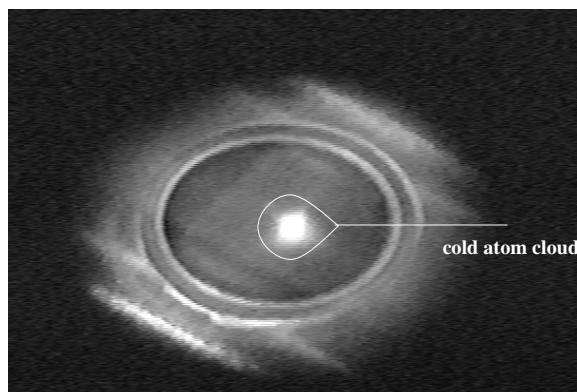


Figure 2.41: Picture of the cold cloud in our MOT

Bibliography

- [1] Optics, Light and Lasers, Dieter Meschede, (WILEY-VCH Verlag GmbH & Co., KGaA, Weinheim (2004)).
- [2] K. B. MacAdam, A. Steinbach, C. Wieman, American Journal of Physics **60**, 1098 (1992).
- [3] L. Ricci, M. Weidemuller, A. Hemmerich, C. Zimmermann, V. Vuletic, W. Konig, T.W. Hansch, Optics Communications **117**, 541(1995).
- [4] Patrick McNicholl and Harold J. Metcalf, Applied Optics **24**, 2757(1985) and the references therein.
- [5] C. Wieman and G. Flowers, American Journal of Physics **63**, 317(1995)